Analyst

Accepted Manuscript

ROYAL SOCIETY OF CHEMISTRY

www.rsc.org/analyst

Sniffer-camera for imaging of ethanol vaporization from wine: effect of wine glass shape

Authors

Takahiro Arakawa [a], Kenta Iitani[a,b], Xin Wang [a], Takumi Kajiro[c], Koji Toma [a], Kazuyoshi Yano[c], Kohji Mitsubayashi[a,b]

Affiliations:

[a]Department of Biomedical Devices and Instrumentation, Institute of Biomaterials and Bioengineering, Tokyo Medical and Dental University, 2-3-10, Kanda-Surugadai, Chiyoda-ku, Tokyo, 101-0062, Japan

[b]Graduate school of Medical and Dental Sciences, Tokyo Medical and Dental University, 1-5-45 Yushima, Bunkyo-ku, Tokyo 113-8549, Japan

[c]Graduate School of Bionics, Computer and Media Sciences, Tokyo University of Technology, 1404-1 Katakura, Hachioji, Tokyo 192-0982, Japan

Corresponding author

Kohji MITSUBAYASHI is a professor at Department of Biomedical Devices and Instrumentation, Institute of Biomaterials and Bioengineering, Tokyo Medical and Dental University, 2-3-10 Kannda-Surugadai, Chiyoda-ku, Tokyo 101-0062, Japan, Phone: + 81-3-5280-8091, Fax: +81-3-5280-8094, E-mail: m.bdi@tmd.ac.jp

Abstract

A two-dimensional imaging system (Sniffer-camera) for visualizing the concentration distribution of ethanol vapor emitting from wine in a wine glass has been developed. This system provides image information of ethanol vapor concentration using chemiluminescence (CL) from an enzyme-immobilized mesh. This system measures ethanol vapor concentration as CL intensities from luminol reactions induced by alcohol oxidase and a horseradish peroxidase (HRP)-luminol-hydrogen peroxide system. Conversion of ethanol distribution and concentration to two-dimensional chemiluminescence was conducted using an enzyme-immobilized mesh containing an alcohol oxidase, horseradish peroxidase, and luminol solution. The temporal changes in CL were detected using an electron multiplier (EM)-CCD camera and analyzed. We selected three types of glass—wine glass, cocktail glass, and straight glass—to determine differences in ethanol emission caused by the shape effects of the glass. The emission measurements of ethanol vapor from wine in each glass were successfully visualized, with pixel intensity reflecting ethanol concentration. Of

note, a characteristic ring shape attributed to high alcohol concentration appeared near the rim of the wine glass containing 13°C wine. Thus, the alcohol concentration in the center of the wine glass was comparatively lower. The Sniffer-camera was demonstrated to be sufficiently useful for non-destructive ethanol measurement for the assessment of food characteristics.

Keywords; optical imaging; alcohol oxidase; luminol reaction; chemiluminescence; wine glass

1. Introduction

Recently, consumers worldwide have been interested in information on food products and beverages such as aroma, safety, characteristics, and quality [1, 2]. In particular, humans have been drinking and tasting wine since ancient times, which is essentially nutty and aromatic but can consist of a variety of smells and tastes [3,4]. Many analytical methods have been reported for the characterization of wine as well as juice, fruit, and other alcoholic beverages [5-8]. Measuring and monitoring ethanol vapor from alcoholic beverages, foodstuffs, and pharmaceutical products is useful in evaluating the extent of maturation during food and drink production [9-12]. The qualities of foods and drinks have been estimated using optical sensors, gas chromatography, semiconductor sensors, and other methods [13-17]. While the human nose can recognize up to 10,000 distinct odors, it is difficult for the general public to identify the odor of food products without special olfactory abilities [18]. Thus, in food analysis, volatile organic compounds (VOCs) emitted from food products represent critical components for food selection, and these can be examined

with sensors, detection devices, and chemical analysis [19, 20]. Various VOCs such as methanol, ethanol, acetaldehyde, hexane, and 2-phenylethanol derived from some foods and beverages can be identified by gas chromatography, mass spectroscopy, and sensory analysis [20-23]. However, these methods are time consuming and require destructive testing and large-scale equipment. Moreover, the concentration and distribution of these VOCs vary temporally and spatially. Therefore, simple, rapid, and non-destructive methods are essential to characterize the odors from food products.

Gas chromatography and gas chromatography–mass spectroscopy have recently attracted attention as useful and precise methods for identifying different gaseous organic compounds. Highly sensitive and selective detection has been achieved for many chemical species using these tools. However, the equipment necessary is expensive and large. These machines are also not suitable for the determination of real-time changes and concentration distribution. For this, continuous and easy monitoring of the spatial behavior of various gas components is required. Some technology employing enzymatic reactions has

been developed in the form of gas sensors—such as biochemical gas sensors for ethanol, acetaldehyde, and various other VOCs—that are based on an NADH-dependent fiber-optic biosensor [24,25]. These enzyme-based biosensors are highly selective and sensitive for target chemicals in food analysis. In addition, chemiluminescence (CL) is a significant method in the field of analytical chemistry [26]. CL does not require other ultra-violet or visible light irradiation, which enables downsizing and simplification of the detection system.

We apply alcohol oxidase (AOD), which catalyzes the conversion of low molecular weight alcohols with molecular oxygen into aldehydes and hydrogen peroxide. This allows for the production and analysis of CL using a horseradish peroxidase (HRP)-luminol-H_2O_2 system. The CL generated by this catalytic reaction is stimulated by the ethanol vapor from wine, and can be imaged and analyzed with an imaging system. In this way, imaging of the concentration distribution of ethanol vapor from wine is demonstrated using a CL reaction.

2. Experimental setup

Experimental procedure for imaging

A cotton mesh (100% cotton, thickness 1 mm, interval size 1 mm) was used for enzyme stabilization. AOD (E.C.1.1.3.13, A2404-1kU, 10–40 units/mg protein, from *Pichia pastoris*, Sigma-Aldrich Co., USA), HRP (E.C.1.11.1.7, 169-10791, 100 units/mg, Wako Pure Chemical Industries, Ltd., Japan), and photo-crosslinkable poly(vinyl alcohol) containing stilbazolium groups (PVA-SbQ, type SPH, 9C-10L, 10.4 wt%, Toyo Gosei Co., Ltd., Japan), were used for enzyme immobilization. A 5.0 mmol/l luminol (01253-60, Kanto Chemical CO., Inc., Japan) solution was prepared in a Tris-HCl buffer solution (100 mmol/l) for measurement of the CL generated by ethanol. These solutions were prepared in deionized distilled water using a Milli-Q purification system (Millipore Co., USA). The solution was stable when stored in the dark. The CL analysis system was constructed with an electron multiplier (EM)-CCD camera (L3C95-05, e2v technologies limited, UK) and a video encoder. Imaging analysis of CL was conducted using Cosmos 32 software (Library Inc., Japan).

Optical imaging system for ethanol from wine

The system for imaging ethanol vapor from a glass of wine was constructed as shown in Fig.1. AOD/HRP-immobilized substrates were prepared with PVA-SbQ with a volume to weight ratio of 1:2. The mixture of enzyme and PVA-SbQ was coated and spread onto a mesh substrate, then cured, and treated with ultraviolet radiation. The size of the mesh substrate was 8 x 8 cm^2. The enzyme-immobilized mesh was stored at 4°C for 4 hours. Together, AOD and HRP were used to generate the CL signal triggered by gaseous ethanol; Tris-HCl buffer solution was the medium for the AOD-catalyzed reaction. HRP was used to catalyze the CL reaction. Ethanol is oxidized to acetaldehyde and hydrogen peroxide by AOD in the presence of oxygen. The peroxide then reacts with the luminol solution, catalyzed by HRP, generating CL (λ= 460 nm). The reactions are summarized as follows [27]:

$$\text{Ethanol} + O_2 \xrightarrow{\text{AOD}} \text{Acetaldehyde} + H_2O_2 \qquad (1)$$

$$\text{luminol} + H_2O_2 + OH^- \xrightarrow{\text{HRP}} \text{3-aminophthalate} + 2H_2O + N_2 + h\nu \qquad (2)$$

The range of imaging is important to consider in the detection of ethanol

concentration from wine, which can be “which can be higher than 200 ppm. In order to enhance the sensitivity of our system, Tris-HCl buffer solution (0.1 mol/l, pH 9.0) was selected and used for further investigation into measuring ethanol vapor from wine. Fig. 2 shows characteristics of six glasses: Riesling wine glass, Pinot Noir wine glass, Cabernet Sauvignon wine glass, a cocktail glass, a standard wine glass, and a straight glass. We selected Japanese red wine (Delica Maison, Suntory Holdings Limited, Japan) and a wine glass (Vinum XL, Riesling Grand Cru, Riedel, Tiroler Glashütte GmbH, Austria) for ethanol vapor imaging.

3. Results and discussion

Evaluation of the ethanol vapor imaging system

The enzyme-immobilized substrate was saturated with concentration-adjusted luminol solution and installed in a dark box in preparation for CL measurement. A UV irradiation time of 5 minutes at low power was used for immobilization of the enzymes onto the mesh substrate using PVA-SbQ. These conditions were optimized to reduce functional damage to the AOD and HRP proteins. The AOD- and-HRP immobilized mesh substrates were evaluated by measuring their response to varying concentrations of gaseous ethanol injected into the imaging system (system detailed in a previous work [28, 29]). Standard gaseous ethanol was injected at a flow rate of 200 ml/min for 20 seconds. The pH 10.3 luminol solution was highly sensitive to ethanol vapor, however calibration range was narrow from 10 to 200 ppm ethanol vapor [30]. The pH 9.0 luminol solution was selected for a wide calibration range of imaging to visualize high concentrations of ethanol vapor. Intensity changes for various concentrations of standard gaseous ethanol were achieved (Fig.3). The insets of

Fig. 3 show images of CL intensity peaks at each concentration of ethanol vapor at 300 and 800 ppm. These images indicate that the gradation of CL relates to the concentration distribution of ethanol vapor on the mesh substrate. The average intensity of CL rapidly increased following the injections of standard ethanol vapor, with peaks appearing at 30 seconds, then gradually decreasing until 120 seconds at 100 ppm ethanol vapor. CL average intensities were related to the concentration of ethanol vapor over the range of 50 to 800 ppm with a correlation coefficient of 0.994. The total volume of each sample of standard gaseous ethanol was 66 mL.

Ethanol vapor imaging of a glass of wine

The direct ethanol vapor imaging system for a wine glass is shown in Fig. 1. This system was designed for easy and simple collection and detection of samples of evaporated ethanol from a glass of wine. We slid the enzyme mesh substrate slowly over the wine glass before imaging to reduce fluctuations of ethanol vapor in the reservoir. The schematic images of the bright-field CCD

image and the original black and white image recorded by the CCD camera are shown in Fig. 4. The 2-D color profile and 3-D profile were analyzed by image analysis software. The 2-D color intensity profile was analyzed from the top of the glass, and the 3-D color intensity profile was converted with the bright-field image and 2-D color profile at an angle of 30 degrees. The Z-axis of the 3-D profile represents CL intensity, or the concentration distribution of evaporated ethanol. Since we adapted an 8-bit EM-CCD camera for this experiment, concentration could be expressed over 256 different colors. In this way, the measurement of ethanol vapor emissions from the wine was successfully visualized, with the intensity of each pixel reflecting ethanol concentration distribution.

Effect of temperature on ethanol vapor distribution

Wine temperature is very important for tasting and smelling the aroma when we drink. In general, a sommelier serves a wine at a specific optimal temperature based on the brand and type of wine. We selected and evaluated

wine at 13°C and 24°C for imaging the concentration distribution of evaporated ethanol. We poured a 100 ml sample of wine at each temperature into separate wine glasses, and waited for the temperatures to stabilize. As before, we slid the enzyme mesh substrate slowly over the wine glass. CL intensity rapidly increased thereafter (Supplemental Movie 1). Fig. 5 shows 2-D color profiles, 3-D profiles, and cross-sectional intensity distributions of ethanol vapor from wine at 13°C and 24°C, with images captured at 20 seconds and 10 seconds after imaging, respectively. A characteristic ring shape appeared near the rim of the glass at 13°C. It was thus assumed that ethanol vapor concentration of the wine at the rim of the glass was in the hundreds of ppm. The intensity profile at the center of the glass at 13°C was 50% weaker than the intensity at the rim of the glass. In contrast, 24°C wine did not exhibit the characteristic ring shape; a high concentration of ethanol vapor appeared over the whole surface of the wine glass. Figure 6 shows time-intensity relation of ethanol vapor from wine at 13°C and 24°C wine in wine glass. The intensity of 24°C wine was rapidly increased at the area of edge and center of glass, which intensity was almost the same

concentration. Conversely, the intensity of 13°C wine was gradually increased, and the concentration at the edge of wine glass was 2 times higher than one of the center of wine glass. Fig. 7 shows characteristic ring shapes of three wine glass of Riesling, Pinot Noir and Cabernet Sauvignon wine glass. The characteristic ring shapes appeared individually at the rim of the each glass. The diameter of these ring were peak width at half-height of intensity. The diameter of ring shape of Cabernet Sauvignon wine glass was much larger than other glass.

Ethanol vapor imaging of different glass shapes

Ethanol vapor imaging of wine in three types of glass is shown in Fig. 8. A cocktail glass, standard wine glass, and straight glass were evaluated for ethanol vapor imaging. The concentration distribution from the cocktail glass and straight glass were high regardless of glass shape and temperature. The characteristic ring shape of ethanol vapor did not appear except in the wine glass at the optimal wine temperature.

Fig. 8 shows the average intensity profiles at the center and edge of the

wine glass at temperatures of 13°C, 24°C, and 30°C. Ethanol vapor from wine at 24°C and 30°C rapidly increased within 10 seconds regardless of measurement point, whereas the intensity only gradually increased at 13°C. The intensity in the center of glass required approximately 50 seconds for a saturated image. Differences in ethanol vapor concentration were estimated to be two-fold at the same temperature.

These results show we can visualize the concentration distribution of ethanol vapor based on the influence of wine temperature at 13°C and 24°C. The alcohol concentration in the center of the wine glass was lower than other areas at 13°C. This phenomenon allows us to smell the aroma of the wine in the center of the glass at a lower alcohol concentration. Accordingly, the shape of wine glass has a very sophisticated and functional design for tasting and enjoying the aroma of wine.

Conclusion

We used alcohol oxidase to catalyze the conversion of low molecular weight alcohols and molecular oxygen into aldehydes and hydrogen peroxide, which can be visualized using the HRP-luminol-H_2O_2 system for ethanol vapor imaging. The temporal changes for various concentrations of ethanol vapor were successfully detected and imaged. The developed method directly imaged ethanol vapor from wine using CL. We established that the characteristic ring shape around the rim of the wine glass, observed at 13°C, is attributable to a higher alcohol concentration near the rim. In future work, this system could be used to image volatile organic compound information from the human body, halitosis, and non-destructive food analysis.

Acknowledgements

We would like to thank Group Gendai Co., Ltd. and RIEDEL (RSN JAPAN Co. Ltd.) for the technical assistance and advice. We would also like to thank the TV show “Einstein's Eye” from the Japan Broadcasting Corporation

(NHK, Nihon Housou Kyoukai). This work is supported in part by the Japan Society for the Promotion of Science (JSPS) Grants-in-Aid for Scientific Research System, by Japan Science and Technology Agency (JST) and by MEXT (Ministry of Education, Culture, Sports, Science and Technology) Special Funds for Education and Research “Research Promotion of Neo-Biology”.

Reference

1. Dion M.A.M. Luykx, Saskia M. van Ruth, An overview of analytical methods for determining the geographical origin of food products, *Food Chemistry*, **107**, 897–911, 2008.
2. J. Saurina, Characterization of wines using compositional profiles and chemometrics, *Trends in Analytical Chemistry,* 29, 3, 234-245, 2010.
3. G. J. Soleas, E. P. Diamandis, D. M. Goldberg, Wine as a biological fluid: history, production, and role in disease prevention, *Journal of Clinical Laboratory Analysis* **11**, 287–313, 1997.
4. J. L. Legras, D. Merdinoglu, J. M. Cornuet, F. Karst, Bread, beer and wine: *Saccharomyces cerevisiae* diversity reflects human history, *Molecular Ecology,* **16**, 2091–2102, 2007.
5. M. Hämmerle, K. Hilgert, M. A. Horn, R. Moos, Analysis of volatile alcohols in apple juices by an electrochemical biosensor measuring in the headspace above the liquid, *Sensors and Actuators B*, **158**, 313–318, 2011.

6. M. A. Ritenour, M. E. Mangrich, J. C. Beaulieu, A. Rab, M. E. Saltveit, Ethanol effects on the ripening of climacteric fruit, *Postharvest Biology and Technology*, 12, 35-42, 1997.

7. S. Oshita, K. Shima, T. Haruta, Y. Seo, Y. Kawagoe, S. Nakayama, H. Takahara, Discrimination of odors emanating from 'La France' pear by semi-conducting polymer sensors, *Computers and Electronics in Agriculture*, **26**, 209–216, 2000.

8. J. A. Pino, S. Tolle, R. Gök, P. Winterhalter, Characterisation of odour-active compounds in aged rum, *Food Chemistry*, **132**, 1436–1441, 2012.

9. W. Tesfaye, M.L. Morales, M.C. Garcı ́a-Parrilla and A.M. Troncoso, Wine vinegar: technology, authenticity and quality evaluation, *Trends in Food Science & Technology*, **13**, 12–21, 2002.

10. Z. G. Cerovic, N. Moise, G. Agati, G. Latouche, N. B. Ghozlen, S. Meyer, *Journal of Food Composition and Analysis*, 21, 650– 654, 2008.

11. C. Steffens, E. Franceschi, F.C. Corazza, P.S.P. Herrmann Jr., J. V. Oliveira, Gas sensors development using supercritical fluid technology to detect the ripeness of bananas, *Journal of Food Engineering*, **101**, 365–369, 2010.

12. B. Kuswandi, R. Andresa, R. Narayanaswamy, Optical fibre biosensors based on immobilisedenzymes, *Analyst*, **126**, 1469-1491, 2001.

13. E. Rijke, P. Out, W. M. A. Niessen, F. Ariese, C. Gooijer, U. A. Th. Brinkman, Analytical separation and detection methods for flavonoids, *Journal of Chromatography A*, 1112, 1-2, 31-63, 2006.

14. A. Zygler, A. Wasik, J. Namieśnik, Analytical methodologies for determination of artificial sweeteners in foodstuffs, *TrAC Trends in Analytical Chemistry*, **28**, 9, 1082-1102, 2009.

15. Z. Pan, L. Wang, W. Mo, C. Wang, W. Hu, J. Zhang, Determination of benzoic acid in soft drinks by gas chromatography with on-line pyrolytic methylation technique, *Analytica Chimica Acta*, 545, 2, 218-223, 2005.

16. Y. Wu, S. Zhang, N. Na, X. Wang, X. Zhang, A novel gaseous ester sensor utilizing chemiluminescence on nano-sized SiO2, *Sensor Actuator B Chem,* **126**(2), 461-466, 2007.

17. A. I. Zia, M. S. A. Rahman, S. C. Mukhopadhyay, P. L. Yu, I.H. Al-Bahadly, C. P. Gooneratne, J. Kosel, T. S. Liao, Technique for rapid detection of phthalates in water and beverages, *Journal of Food Engineering*, **116**, 2, 515-523, 2013.

18. E. Schaller, J. O. Bosset, F. Escher, 'Electronic noses' and their application to food, *LWT - Food Science and Technology*, **31**, 4, 305-316, 1998.

19. D. Kohl, Function and applications of gas sensors, *Journal of Physics D: Applied Physics,* **34**, 19, R125-R149, 2001.

20. D. James, S. M. Scott, X. Ali, W. T. O'Hare, Chemical sensors for electronic nose systems, *Microchimica Acta*, **149**, 1-2, 1-17, 2005.

21. C, Elosua, I. R. Matias, C. Bariain, F. J. Arregui, Volatile organic compound optical fiber sensors: A review, *Sensors*, **6**, 11 1440-1465, 2006.

22. B. Culshaw, G. Stewart, F. Dong, C. Tandy, D. Moodie, Fibre optic techniques for remote spectroscopic methane detection - From concept to system realisation, *Sensors and Actuators, B: Chemical*, **51**, 1-3, 25-37, 1998.

23. S. Christie, E. Scorsone, K. Persaud, F. Kvasnik, Remote detection of gaseous ammonia using the near infrared transmission properties of polyaniline, *Sensors and Actuators, B: Chemical*, **90**, 1-3, 163-169, 2003.

24. K. Mitsubayashi, G. Nishio, M. Sawai, T. Saito, H. Kudo, H. Saito, K. Otsuka, T. Noguer, and J. L. Marty, A bio-sniffer stick with FALDH (formaldehyde dehydrogenase) for convenient analysis of gaseous formaldehyde, *Sensors and Actuators, B: Chemical*, **130**, 1, 32-37, 2008.

25. H. Kudo, M. Sawai, X. Wang, T. Gessei, T. Koshidad, K. Miyajima, H. Saito, and K. Mitsubayashi, A NADH-dependent fiber-optic biosensor for ethanol determination with a UV- LED, *Sensors and Actuators, B: Chemical*, **141**, 1, 20–25, 2009.

26. M. L. Liu, Z. Lin, and J. M. Lin, A review on applications of chemiluminescence detection in food analysis, *Analytical Chimica Acta*, **670**, 1-2, 1-10, 2010.

27. P. Fletcher, K. N. Andrew, A. C. Calokerinos, S. Forbes, P. J. Worsfold, Applications of Flow Injection Chemiluminescence Detection - A review, *Luminescence,* **16**, 1-23, 2001.

28. T. Arakawa, X. Wang, T. Kajiro, K. Miyajima, S. Takeuchi, H. Kudo, K. Yano, K. Mitsubayashi, A direct gaseous ethanol imaging system for analysis of alcohol metabolism from exhaled breath, *Sensors and Actuators B*, 186, 27–33, 2013.

29. X. Wang, E. Ando, D. Takahashi, T. Arakawa, H. Kudo, H. Saito, K. Mitsubayashi, Non-invasive spatial visualization system of exhaled ethanol for real-time analysis of ALDH2 related alcohol metabolism, *Analyst*, **136**(18), 3680-3685, 2011.

30. T. Arakawa, E. Ando, X. Wang, K. Miyajima, H. Kudo, H. Saito, T. Mitani, M. Takahashi, K. Mitsubayashi, A highly sensitive and temporal visualization system for gaseous ethanol with chemiluminescence enhancer, *Luminescence*, **27**, 328-333, 2012.

Figure caption

Figure 1. Experimental setup for optical imaging of wine. (a) Fabrication process of the AOD- and HRP-immobilized mesh for imaging using UV cross-linkable PVA-SbQ. (b) This system was composed of wine poured into a wine glass, an immobilized enzyme mesh, and an EM-CCD recoding system.

Figure 2. Experimental setup of six types of glass for ethanol vapor imaging: Riesling wine glass, Pinot Noir wine glass, Cabernet Sauvignon wine glass, a cocktail glass, a standard wine glass, and a straight glass.

Figure 3. Calibration curve of this system for ethanol vapor measurement using pH9.0 and pH10.3 luminol solution. The CL intensities detected with optical imaging were related to the concentrations of ethanol vapor from 30 to 800 ppm (pH9.0).

Figure 4. Schematic image of the bright-field CCD image and original CCD image. 2-D color profiles and 3-D profiles were analyzed by image analysis software.

Figure 5. 2-D color profiles, 3-D profiles, and cross-sectional intensity distribution of the ethanol vapor from wine showing the influence of wine temperature. (a) Wine glass at 13°C, (b) Wine glass at 24°C. Images were captured at 20 seconds for 13°C and 10 seconds for 24°C.

Figure 6. Temporal changes of evaporated ethanol CL intensity from 13°C and 24°C wine at the center and edge of a wine glass.

Figure 7. 2-D intensity profile of the cocktail glass, wine glass, and straight glass. The concentration distribution of ethanol vapor with the characteristic ring shape appeared at the edge of the wine glass.

Figure 8. Temporal changes of evaporated ethanol CL intensity from wine at the center and edge of a wine glass.

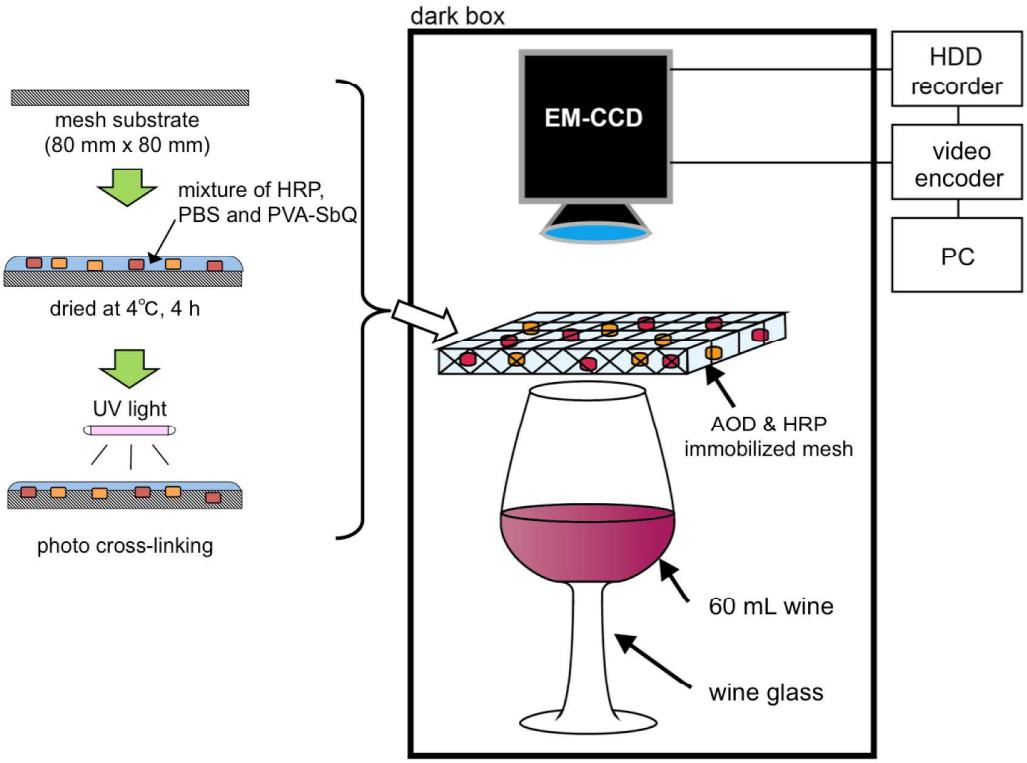

Figure 1

Schematic image of three types of wine glass

	wine glass Riesling	wine glass Pinot Noir	wine glass Cabernet Sauvignon
shape	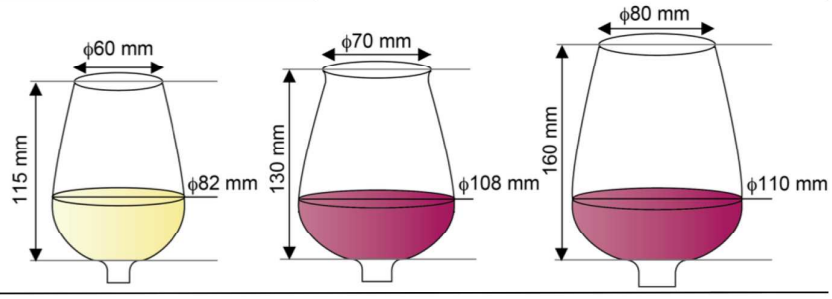		
full volume (mL)	420	780	1000
opening size (mm)	60	70	80

Schematic image of three types of glass

	cocktail glass	wine glass	straight glass
shape	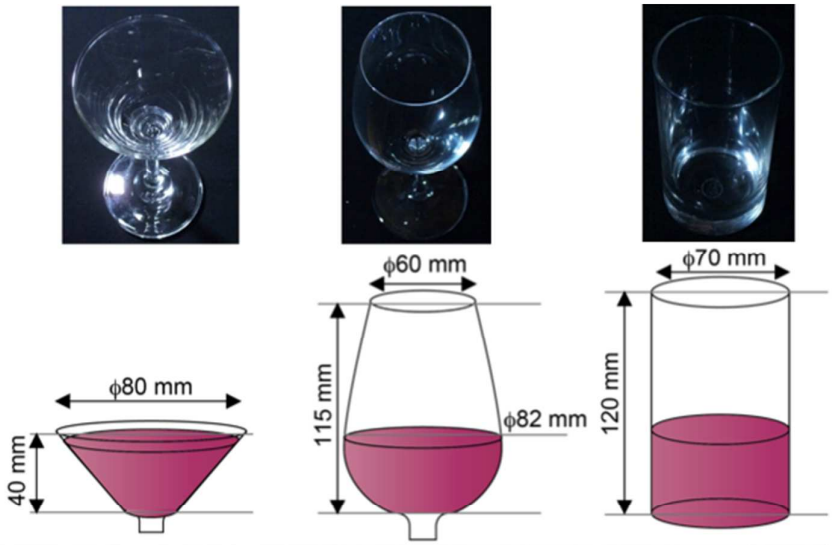		
full volume (mL)	80	420	300
opening size (mm)	80	60	70

Figure 2

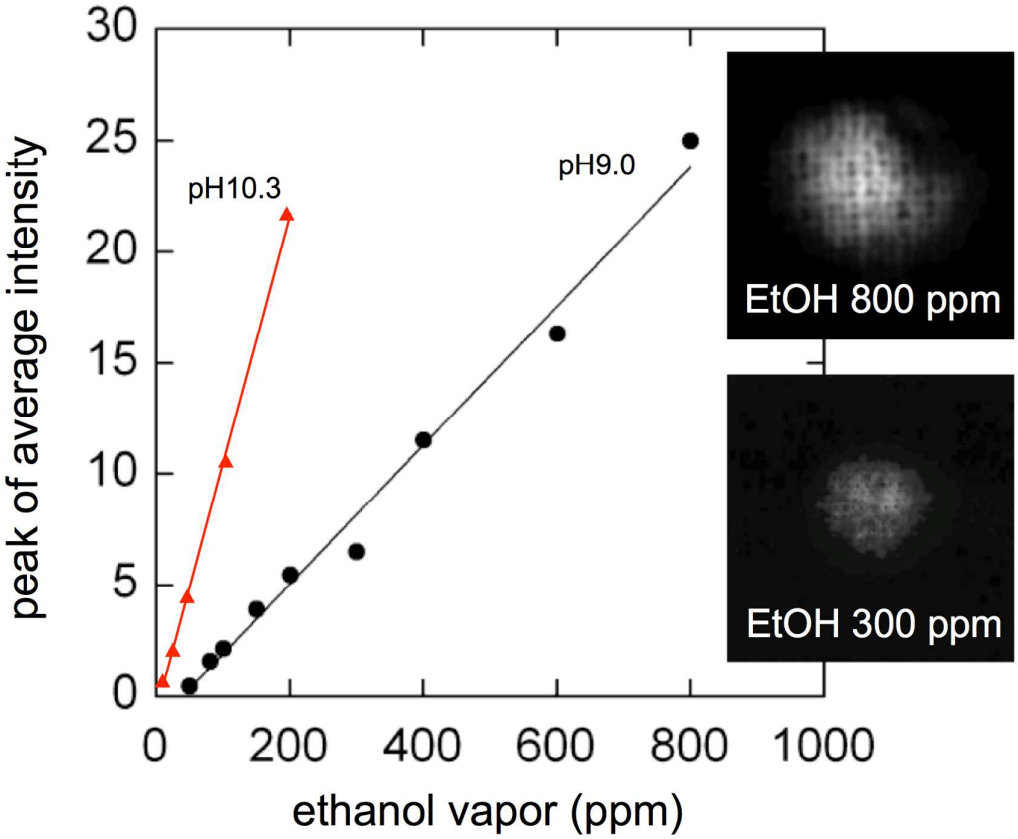

Figure 3

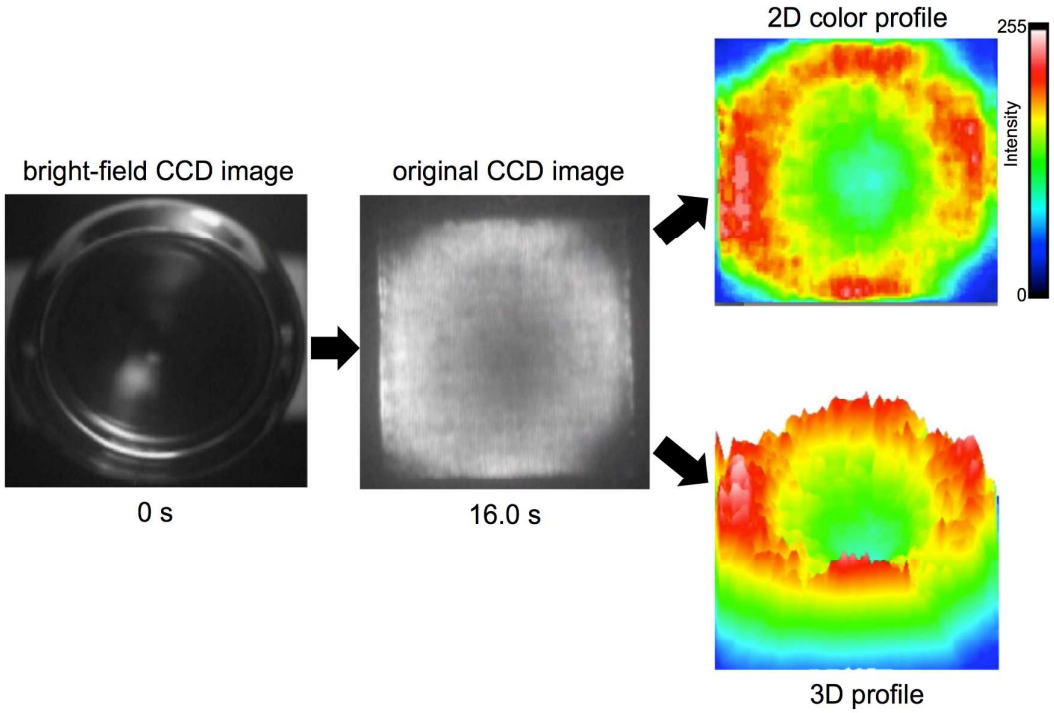

Figure 4

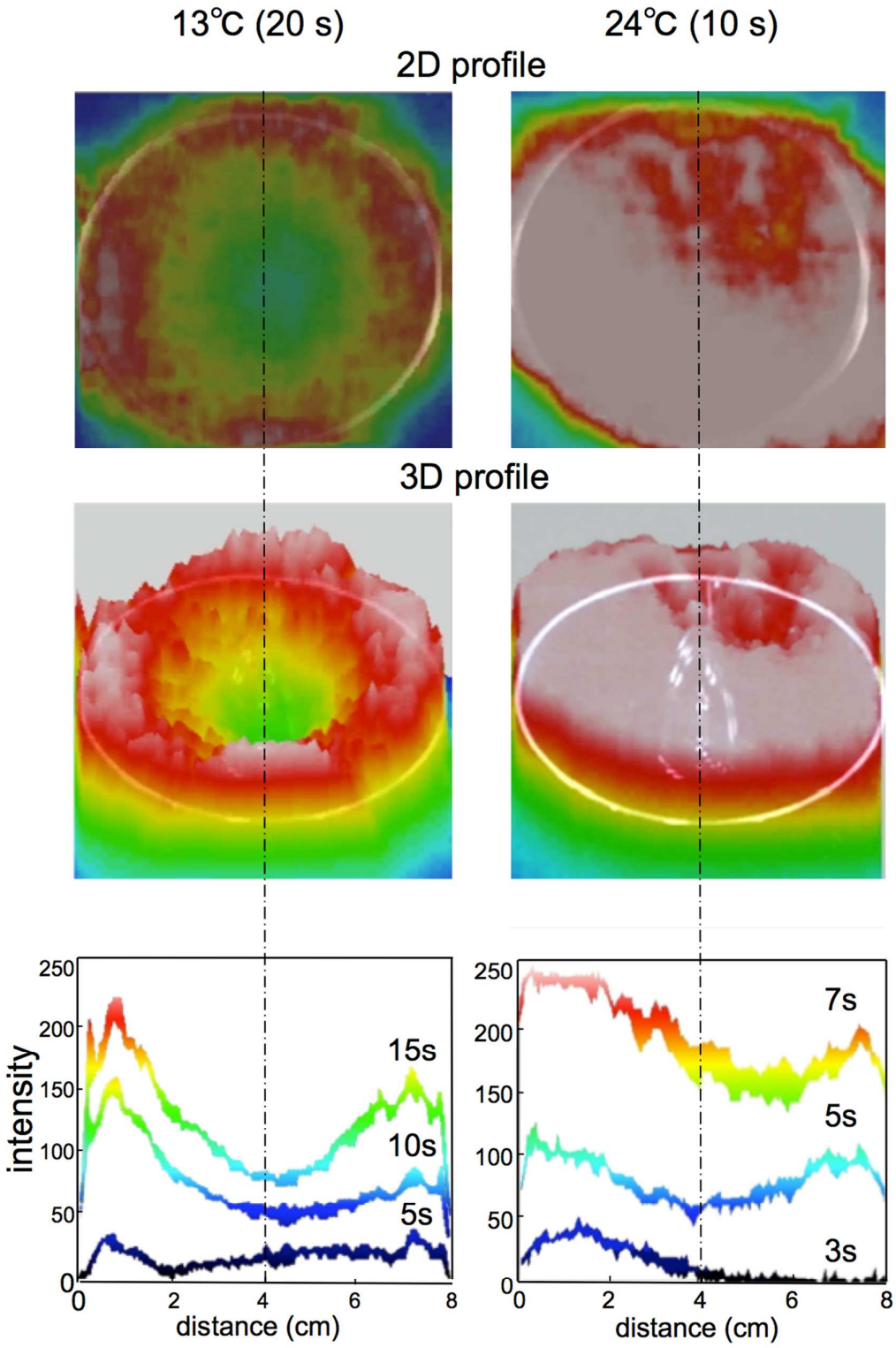

Figure 5

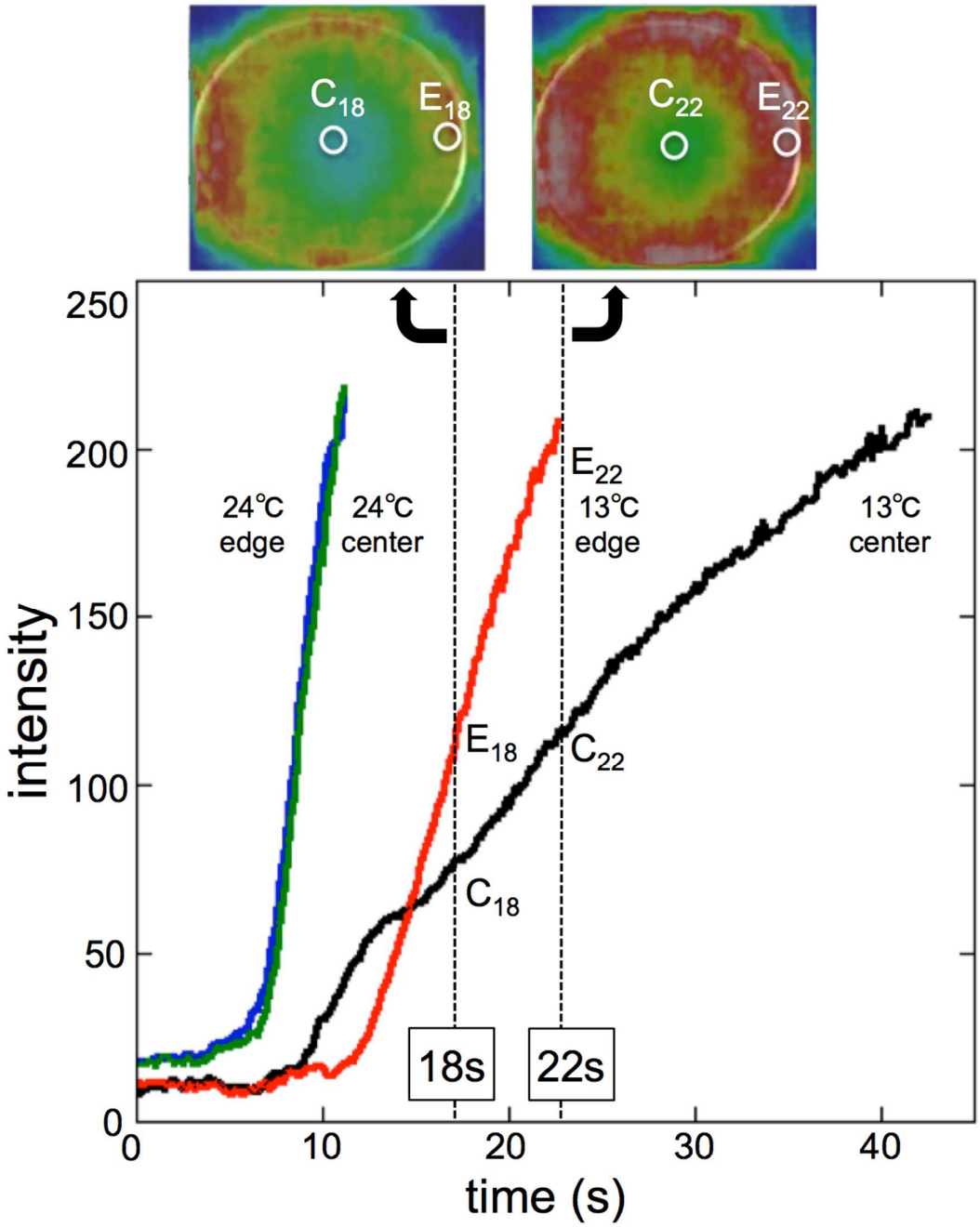

Figure 6

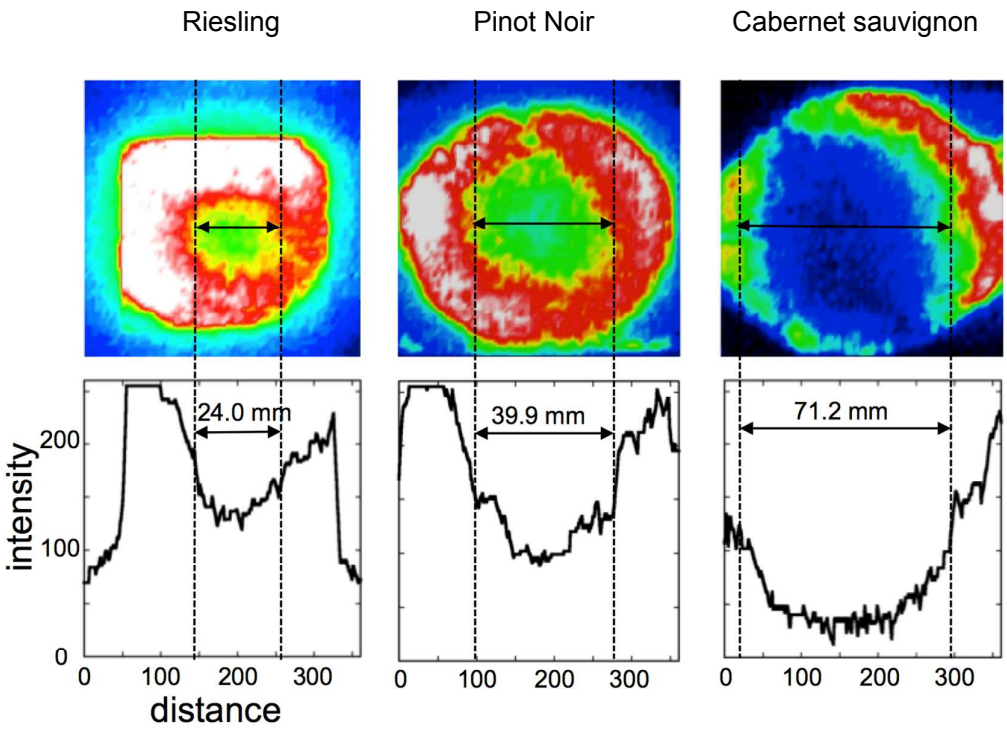

Figure 7

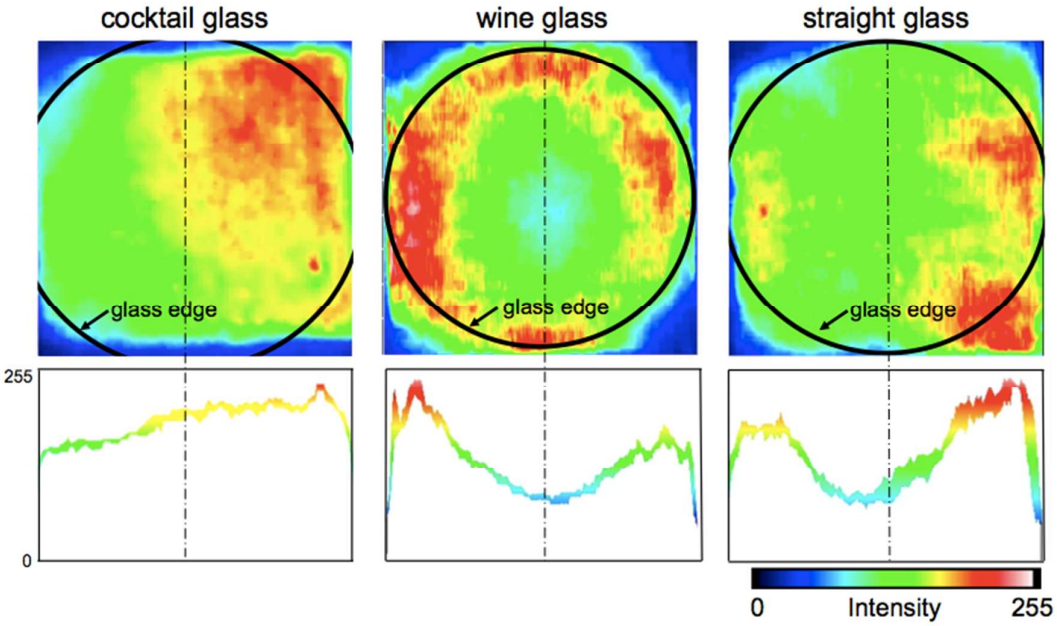

Figure 8

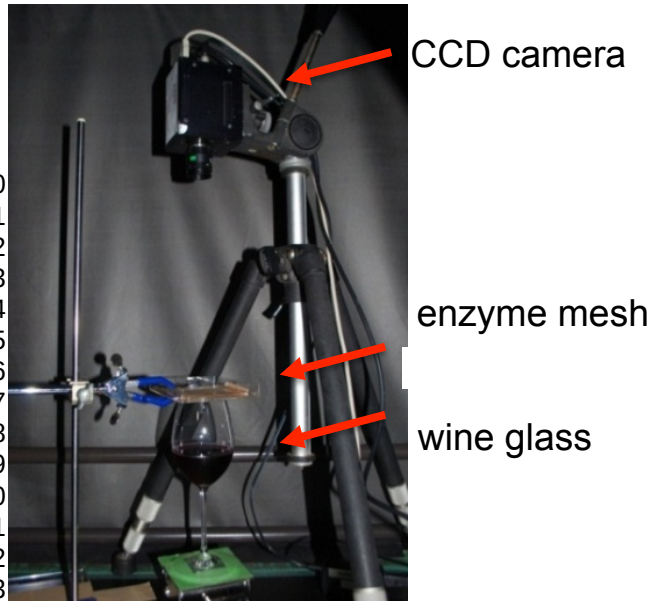

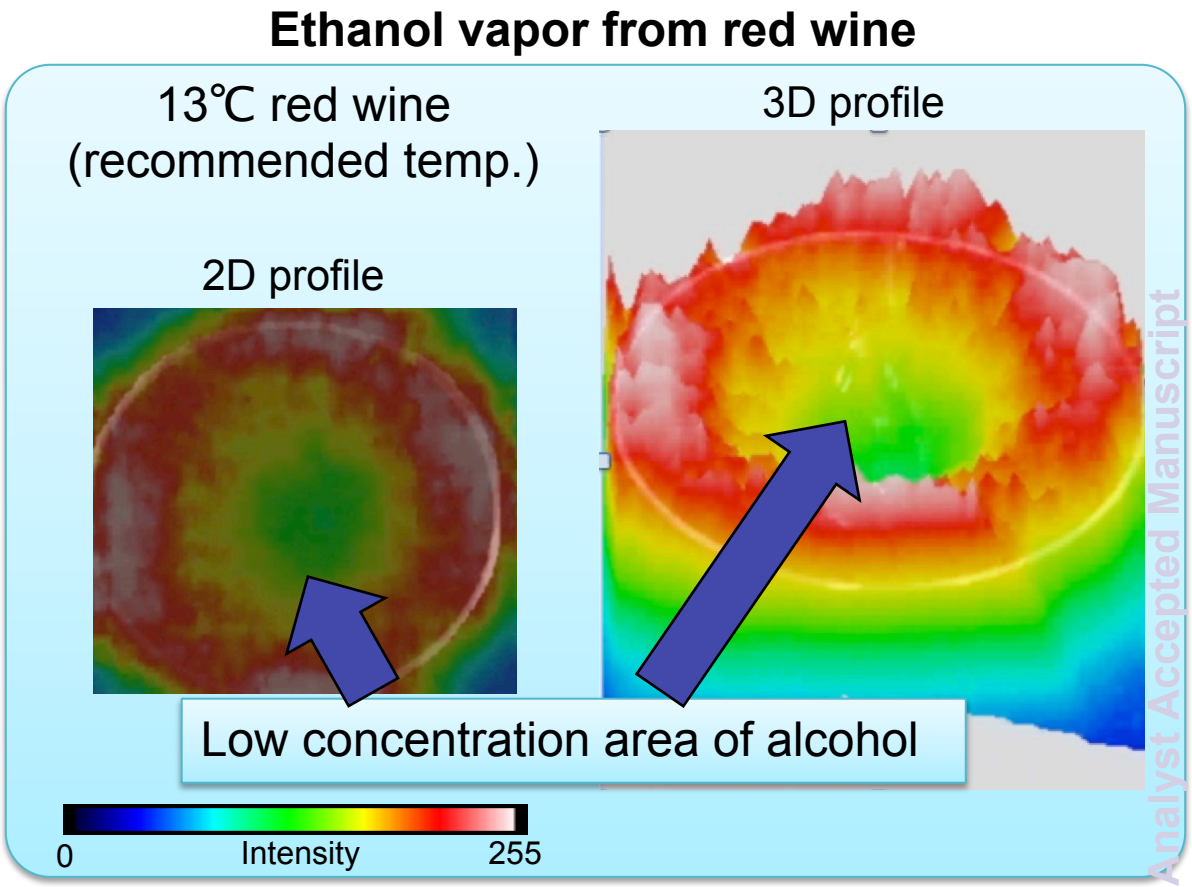

Graphical Abstract

Sniffer-camera for imaging of ethanol vaporization from wine